Supporting Information

Indazole- and Indole-5-carboxamides: Selective and Reversible Monoamine Oxidase B Inhibitors with Subnanomolar Potency

Nikolay T. Tzvetkov,[a,]* *Sonja Hinz,*[a] *Petra Küppers,*[a] *Marcus Gastreich,*[b] *Christa E. Müller*[a,]*

[a]PharmaCenter Bonn, University of Bonn, Pharmaceutical Institute, Pharmaceutical Chemistry I, Bonn, Germany

[b]BioSolveIT GmbH, An der Ziegelei 79, 53575 St. Augustin, Germany

Table of contents

Experimental procedures for the preparation of carboxylic acids **18** and **19** S3–S4
Preparation of 5-chloro-6-morpholinonicotinic acid (**18**) S3
Preparation of 1-methyl-6-oxo-1,6-dihydropyridine-3-carboxylic acid (**19**) S4
NMR spectra of compounds **10** and **11** S5–S6
Figure S1. NMR spectra of **10** S5
Figure S2. NMR spectra of **11** S6
Chromatographic conditions S7–S10
Table S1. LC/ESI-MS data of the target compounds S9
Chemical stability of compounds **54** and **59** S11–12
Figure S3. LC/ESI-MS spectra of **54** S11
Figure S4. LC/ESI-MS spectra of **59** S12
Table S2. Purity of compounds **54** and **59** determined by LC-MS analyses S12
E/Z stereochemistry of compound **58** S13
Figure S5. Lowest energy geometries of *E/Z* isomers of **58** S13
Pharmacological studies S14–S16
Figure S6. Reaction scheme for the determination of MAO-B activity S15
Figure S7. Inhibition curve for compound **15** at rat and human MAO-B S16
Figure S8. Correlation of rat versus human pIC_{50} values at MAO-B S17
Figure S9. Dixon plot for compound **15** S18
Physicochemical profiling of the target compounds S19–S23
Table S3. Calculated physicochemical parameters (Instant JChem) and melting points S19
Table S4. Calculated physicochemical parameters (ACD/ChemSketch) S20
Figure S10. Distribution of the logP values plotted versus M_R, *t*PSA and pIC_{50} values at human MAO-B S21
Table S5. Comparison of suggested and preferred physicochemical property ranges S22
Table S6. Predicted properties of selected compounds as potential CNS drugs S23
Computational analysis S24
Table S7. Superimposition results for safinamide and selected ligands **15** and **28** S24
Figure 11. Compounds **15** and **28** overlaid onto the crystal structure of safinamide S24
References S25–S26

Experimental Procedures for the preparation of carboxylic acids 18 and 19

General

All reagents and solvents were of commercial quality and were used without further purification. The commercially available ethyl 5,6-dichloronicotinate (**A-1**, TCI) and 6-hydroxynicotinic acid (**B-1**, Aldrich) were used as starting materials for the preparation of **18** and **19**, respectively. The purity of the final products was found to be not less than 95% by LC/ESI-MS analyses. Reaction control was done by HPLC with UV-detection on an Agilent 1100 instrument. Melting points were measured on a Büchi B545 apparatus. NMR spectra were recorded on a Bruker Avance 500 MHz spectrometer. The chemical structures were drawn with ChemBioDraw® Ultra V. 13.0.

Preparation of 5-chloro-6-morpholinonicotinic acid (18)[1]

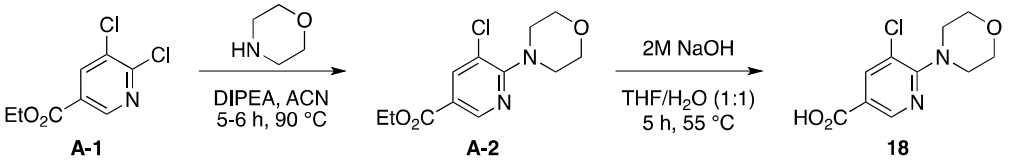

A solution of ethyl 5,6-dichloronicotinate (**A-1**, 1.1 g, 5.0 mmol), *N*,*N*-diisopropylethylamine (DIPEA, 0.97 g, 7.5 mmol) in acetonitrile (3.0 mL) was treated with morpholine (0.48 g, 6.0 mmol). The mixture was stirred for 6 hours at 95 °C. The complete conversion of the starting material could be detected by observing a change of the color from yellowish to deep orange. After complete conversion, the mixture was evaporated to dryness, the residue diluted with water (20 mL), and extracted with dichloromethane (3x20 mL). The combined organic layer was dried over sodium sulfate and evaporated under reduced pressure to yield 1.31 g (97 %) of **A-2** as a red oil. The product was identified by LC/ESI-MS analysis and used for the next synthetic step without further purification.

The ester **A-2** (1.31 g, 4.83 mmol) was dissolved in a tetrahydrofurane/water mixture (1:1, 4.0 mL) and treated with 2.0 *M* sodium hydroxide (0.33 g, 5.80 mmol). The reaction mixture was stirred for 5 h at 55 °C. After complete conversion, the mixture was cooled to room temperature, diluted with water (20 mL) and extracted with ethyl acetate (3x20 mL). The water layer was neutralized with an aqueous solution of hydrochloric acid (2.0 *N*) until a white precipitate was observed. The product was collected by repeated filtration and evaporation. The combined product fractions were dried at 70 °C yielding 1.17 g (100 %) of **18** as a white solid, m.p. 185.2–186.2; ^{1}H NMR (500 MHz, DMSO-d_6) δ (ppm) 3.45 (t, J = 5.04 Hz, 2xCH_2, 4H), 3.72 (t, J = 4.41 Hz, 2xCH_2, 4H), 8.08 (d, J = 1.89 Hz, CH, 1H), 8.66 (d, J = 1.90 Hz, CH, 1H), 13.01 (s, CO_2H, 1H). ^{13}C (125 MHz, DMSO-d_6) δ (ppm) 48.9 (2xCH_2), 66.1 (2xCH_2), 119.4, 139.7, 147.5, 159.3, 165.4; LC/ESI-MS (m/z): 243.28 $[M+H]^+$; Purity: 100.0 % (N).

Preparation of 1-methyl-6-oxo-1,6-dihydropyridine-3-carboxylic acid (19)[2]

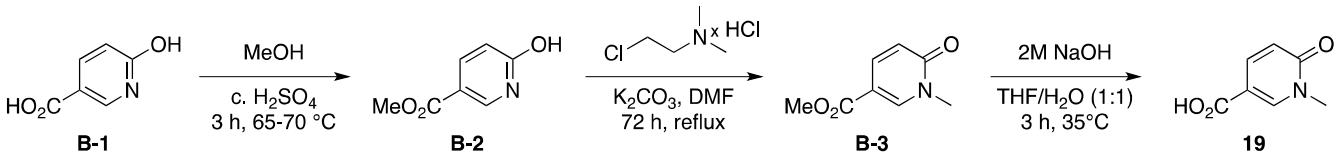

A mixture of 6-hydroxynicotinic acid (**B-1**, 2.48 g, 17.8 mmol) and a catalytic amount of concentrated sulfuric acid (10 mol-%) in methanol (20.0 mL) was heated for 3 h at 65–70 °C. After complete conversion, the mixture was cooled to room temperature and hydrolyzed dropwise with a saturated sodium carbonate solution (20 mL) until the mixture reached pH 11–12. The resulting mixture was extracted with ethyl acetate (3x20 mL). The combined organic layer was dried over sodium sulfate, filtered and the solvent removed under reduced pressure to afford 2.70 (99 %) of **B-2** as a white crystalline solid; ^{1}H NMR (500 MHz, DMSO-d_6) δ (ppm) 3.86 (s, CO_2Me, 3H), 6.38 (d, J = 8.82 Hz, CH_{aromat}, 1H), 7.86 (dd, J = 1.89 / 8.83 Hz, CH_{aromat}, 1H), 8.04 (s, CH, 1H), 12.03 (br. s, OH, 1H). The product **B-2** was used for the next synthetic step without further purification.

A solution of the nicotinic acid methyl ester (**B-2**, 347 mg, 2.27 mmol), potassium carbonate (376 mg, 2.72 mmol) in dry *N*,*N*-dimethylformamide (DMF, 3.0 mL) was treated with 2-*N*,*N*-dimethylaminoethyl-chloride hydrochloride (392 mg, 2.72 mmol) and the reaction mixture was stirred at for 72 h at 95 °C. After complete conversion, the reaction mixture was cooled to room temperature, diluted with ethyl acetate (5.0 mL), filtered, and washed with water (3x10 mL). The organic layer was dried over sodium sulfate and evaporated under reduced pressure (32 mbar, 75°C). The residue was purified by column chromatography on silica gel (eluent: dichloromethane/methanol, 9:1 or 9.5:0.5, v/v). The product was additionally re-crystallized from ethyl acetate/*n*-hexane to obtain methyl 1-methyl-6-oxo-1,6-dihydropyridine-3-carboxylate (**B-3**, 125 mg, 33%) as a beige-brownish solid; ^{1}H NMR (500 MHz, DMSO-d_6) δ (ppm) 3.50 (s, CH_3, 3H), 3.78 (d, J = 5.20 Hz, CH_3, 3H), 6.42 (d, J = 9.50 Hz, CH, 1H), 7.79 (dd, J = 2.61 / 9.50 Hz, CH, 1H), 8.53 (d, J = 2.51 Hz, 1H). ^{13}C (125 MHz, DMSO-d_6) δ (ppm) 37.7 (Me), 52.1, 118.7, 120.0, 138.5, 146.2, 164.2, 168.1.

The methyl ester **B-3** (111 mg, 0.67 mmol) was dissolved in a tetrahydrofurane/water mixture (1:1, 2.0 mL), treated with 2.0 *M* sodium hydroxide (32.2 mg, 0.80 mmol) and the mixture was stirred for 3 h at 35 °C. After complete conversion, the cooled reaction mixture was diluted with water (10 mL) and extracted with ethyl acetate (3x10 mL). The aqueous layer was acidified to pH 2-3 by dropwise adding of an aqueous solution of hydrochloric acid (1.0 *N*). The precipitate formed was collected by repeated cooling at 0-5 °C (ice-water-bath) and subsequent filtration. The white crystalline product was re-crystallized from ethyl acetate/*n*-hexane to obtain 101 mg (99%) of **19** as a beige-colored solid, m.p. 233.4–234.4 °C (dec.); ^{1}H NMR (500 MHz, DMSO-d_6) δ (ppm) 3.48 (s, CH_3, 3H), 6.39 (d, J = 9.46 Hz, CH, 1H), 7.76 (dd, J = 2.53 / 9.46 Hz, CH, 1H), 8.45 (d, J = 2.52 Hz, 1H), 12.7 (br. s., CO_2H, 1H). ^{13}C (125 MHz, DMSO-d_6) δ (ppm) 37.4 (N-Me), 109.1, 118.2, 138.9, 145.0, 162.1, 165.5; LC/ESI-MS (m/z): 154.24 $[M+H]^+$; 152.18 $[M-H]^-$; Purity: 96.49 % (N).

Note that the alkylation of nicotinic acid methyl ester (**B-2**) with 2-*N*,*N*-dimethylaminoethyl-chloride hydrochloride under the above mentioned reaction conditions led to the formation of the by-product methyl 1-(2-(dimethylamino)ethyl)-6-oxo-1,6-dihydropyridine-3-carboxylate (not showed on the scheme above) in a 6 : 1 ratio with **B-3**. Both compounds were separated by column chromatography on silica gel as described. Compound **B-3** is the major product formed via an alkylation and subsequently rearrangement reaction. To achieve a maximum conversion of the starting material the reaction was monitored by HPLC-UV.

NMR spectra of compounds 10 and 11

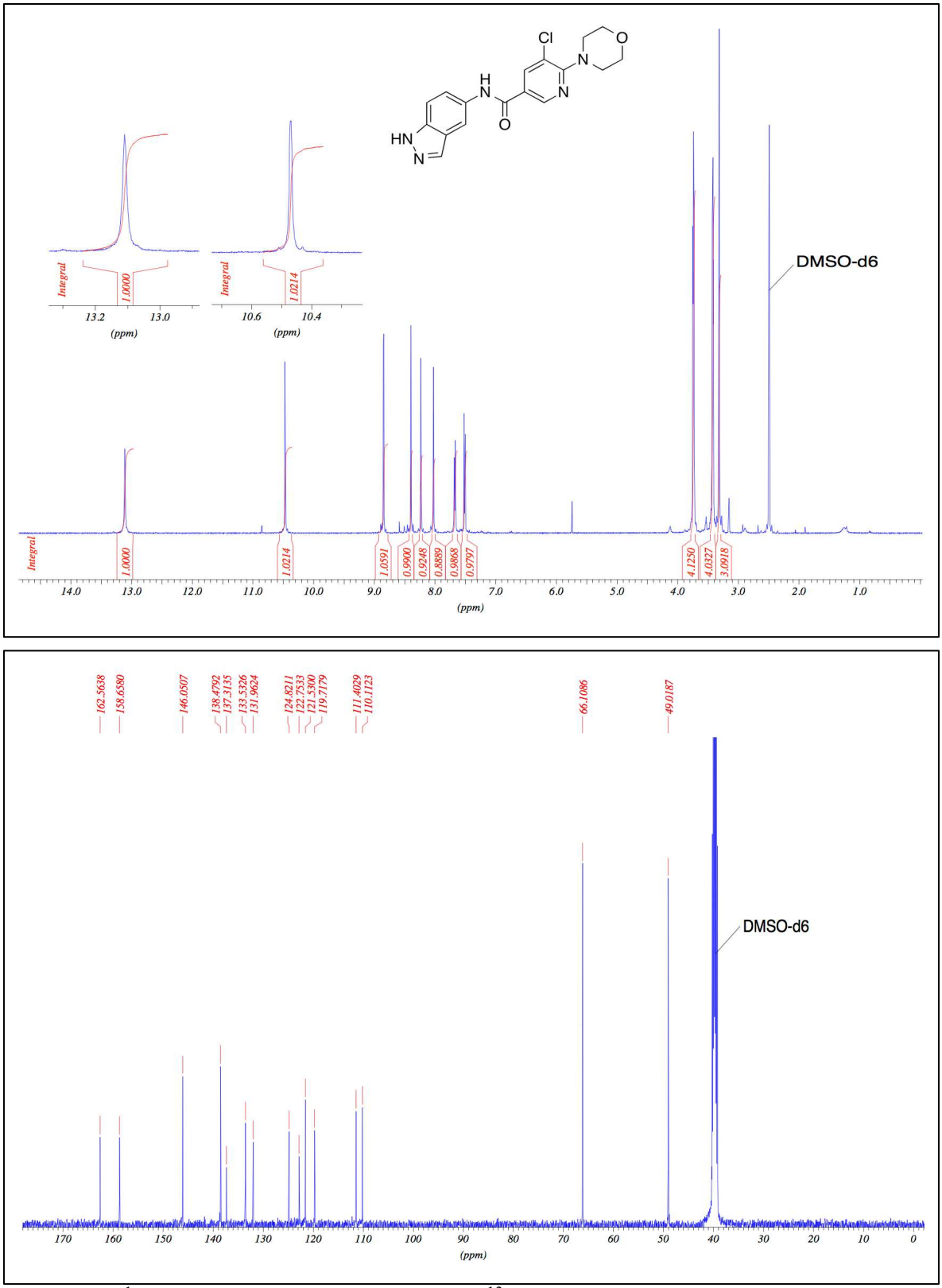

Figure S1. ^{1}H-NMR at 500.13 MHz (top) and ^{13}C-NMR spectra at 125.76 MHz (bottom) of compound **10**. Both spectra were measured in DMSO-d_6 at room temperature (303 K).

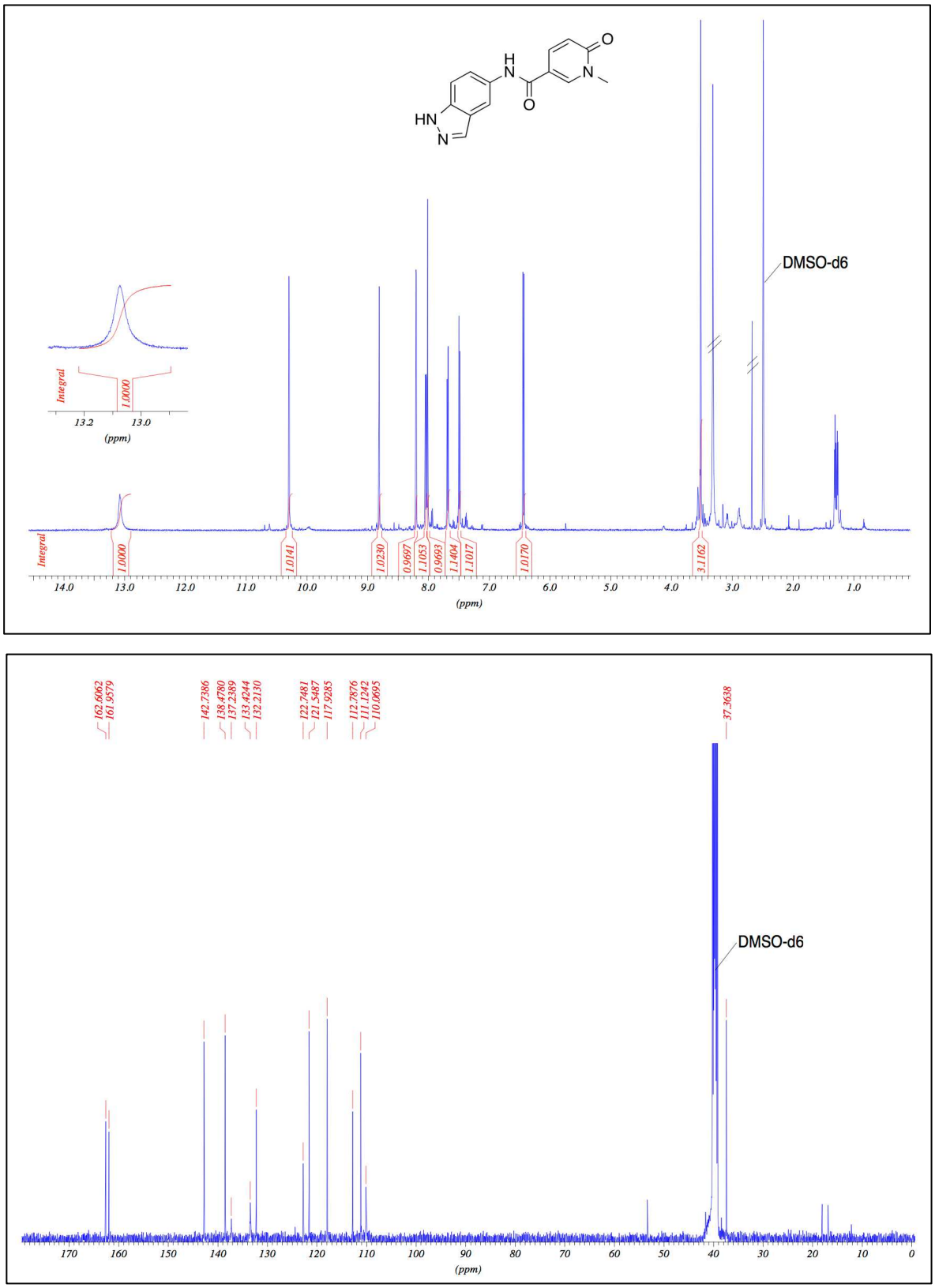

Figure S2. ^{1}H-NMR at 500.13 MHz (top) and ^{13}C-NMR spectra at 125.76 MHz (bottom) of compound **11**. Both spectra were measured in DMSO-d_6 at room temperature (303.3 K).

Chromatographic conditions

The purity of the target compounds was determined by HPLC-UV using an LC-MS instrument (Applied Biosystems API 2000 LC/ESI-MS, HPLC Agilent 1100 system from Agilent Technologies, Böblingen, Germany) using a diode array detector (DAD) with a UV absorption range from 220 to 400 nm. Mass spectra were recorded on an API 2000 mass spectrometer (Applied Biosystems, Darmstadt, Germany) equipped with an electrospray ion source (ESI) by using alternating positive (+Q) and/or negative (-Q) ion triple quadrupole with a scan speed up to 2400 amu/sec. Methanol from Sigma-Aldrich (Chromasolv® LC-MS grade) with ammonium acetate (2.0 mM) and water Purelab flex (ELGA Labwater, UK) were used as LC mobile phases.

Preparation procedure of the test samples for LC/ESI-MS analyses

The target compounds were dissolved at a concentration of 1.0 mg/mL in methanol and if necessary sonicated for two hours to complete dissolving. If required, samples were filtered through a Chromafil® filter (0.45 µm, Macherey & Nagel) into the 1.0 mL HPLC glass vials in order to separate dissolved from particulate material directly prior to injection. Then 5.0 µL of the compound solution was injected into a NUCLEODUR C18 Gravity (50 × 2.0 mm, particle size 3.0 µM) analytical HPLC column (Macherey & Nagel, Düren, Germany) and elution was performed with a standard gradient of water (Solvent A) : methanol (Solvent B) containing 2.0 mM ammonium acetate (neutral, pH 7.4 ± 0.2) starting from 60 : 40 (A/B) to 0 : 100 (A/B) for 10 min with a total run time of 20 min and a flow rate of 300 µL/min (standard method).

Standard LC/ESI-MS method for quality/purity control of tested new and reference compounds

Agilent 1100 binary pump and thermostat settings:
Solvent A: water + 2.0 mM ammonium acetate
Solvent B: methanol + 2.0 mM ammonium acetatte

Gradient

Total Time (min)	Solv. A (%)	Solv. B (%)	Flow Rate (µL/min)
10.00	60	40	300
0.02	60	40	300
10.00	0.0	100	300
20.00	0.0	100	300

Stop time: 20.2 min

Pressure limits (bar):
Minimum pressure: 0
Maximum pressure: 600
Run pressure: 120 bar
Column temperature: 25 °C

Detection settings:
UV detection (DAD) range: from 220.0 to 400.0 nm
Full scan mass detection: in positive (+Q) and negative (-Q) mode with 150–180 scans/min

Modified LC/ESI-MS method for quality/purity control of polar/highly soluble compounds

The target compounds were dissolved at a concentration of 1.0 mg/mL in methanol and if necessary sonicated for two hours to complete dissolution. If required, samples were filtered through a Chromafil® filter (0.45 µm, Macherey & Nagel) into the 1.0 mL HPLC glass vials in order to separate dissolved from particulate material immediately prior to injection. Then 10.0 µL of the compound solution was injected into a Phenomenex Luna C18 (50 × 2.0 mm, particle size 3.0 µM) HPLC column (Aschaffenburg, Germany) and elution was performed with a standard gradient of water (solvent A) : methanol (solvent B) either containing 2.0 mM ammonium acetate and 0.1% formic acid (acidic, chrom. system A) or 2.0 mM ammonium acetate (neutral, chrom. system B, pH 7.4 ± 0.2) starting from 90 : 10 (A/B) to 0 : 100 (A/B) for 10 min with a total run time of 30 min and a flow rate of 250 µL/min (modified method).

Agilent 1100 binary pump and thermostat settings:
Solvent A: water + 2.0 mM ammonium acetate
Solvent B: methanol + 2.0 mM ammonium acetate

Gradient

Total Time (min)	Solv. A (%)	Solv. B (%)	Flow Rate (µL/min)
10.00	90	10	250
0.02	90	10	250
10.00	0.0	100	250
30.00	0.0	100	250

Stop time: 30.2 min

Pressure Limits (bar):
Minimum pressure: 0
Maximum pressure: 600
Run pressure: 120 bar
Column temperature: 25 °C

Detection settings:
UV detection (DAD) range: from 220.0 to 400.0 nm
Full scan mass detection: in positive (+Q) and negative (-Q) mode with 150–180 scans/min

Table S1. LC/ESI-MS data of the target compounds.

Compd	Mass calculated for	Exact Mass m/z	Mass full scan		UV detection	Purity
			$[M+H]^+$	$[M-H]^+$		
10	$C_{17}H_{16}ClN_5O_2$	357.10	358.21	356.27	DAD (λ_{max} = 252 nm)	96.9 %
11	$C_{14}H_{12}N_4O_2$	268.10	269.16	267.17	DAD (λ_{max} = 266 nm)	99.3 %
12	$C_{14}H_9ClFN_3O$	289.04	290.33	288.05	DAD (λ_{max} = 234 nm)	99.1 %
13	$C_{14}H_9Cl_2N_3O$	305.01	306.33	304.00	DAD (λ_{max} = 236 nm)	99.7 %
14	$C_{14}H_9Cl_2N_3O$	305.01	306.36	303.96	DAD (λ_{max} = 236 nm)	96.2 %
15	$C_{14}H_9Cl_2N_3O$	305.01	306.22	304.00	DAD (λ_{max} = 232 nm)	99.5 %
16	$C_{15}H_{11}Cl_2N_3O$	319.03	320.13	318.04	DAD (λ_{max} = 236 nm)	99.5 %
26	$C_{14}H_{11}N_3O$	237.09	238.22	236.19	DAD (λ_{max} = 228 nm)	99.3 %
27	$C_{14}H_9Cl_2N_3O$	305.01	306.33	304.08	DAD (λ_{max} = 230 nm)	95.3 %
28	$C_{14}H_9ClFN_3O$	289.04	290.24	288.05	DAD (λ_{max} = 236 nm)	97.9 %
29	$C_{14}H_9ClFN_3O$	289.04	290.26	288.04	DAD (λ_{max} = 232 nm)	95.5 %
30	$C_{14}H_9F_2N_3O$	273.07	274.31	272.06	DAD (λ_{max} = 236 nm)	98.0 %
31	$C_{16}H_{15}N_3O_3$	297.11	298.47	296.31	DAD (λ_{max} = 226 nm)	100 %
32	$C_{15}H_{12}ClN_3O_2$	301.06	302.21	300.21	DAD (λ_{max} = 232 nm)	95.2 %
33	$C_{14}H_{10}ClN_3O_2$	287.05	288.11	286.11	DAD (λ_{max} = 228 nm)	98.3 %
34	$C_{15}H_{12}ClN_3O_2$	301.06	302.21	300.21	DAD (λ_{max} = 234 nm)	95.3 %
35	$C_{14}H_{10}ClN_3O_2$	287.05	288.11	286.12	DAD (λ_{max} = 228 nm)	95.1 %
36	$C_{13}H_8Cl_2N_4O$	306.01	307.30	305.12	DAD (λ_{max} = 228 nm)	95.2 %
37	$C_{15}H_{11}Cl_2N_3O$	319.03	320.13	318.01	DAD (λ_{max} = 236 nm)	100 %
38a	$C_{15}H_{11}Cl_2N_3O$	319.03	320.06	317.96	DAD (λ_{max} = 236 nm)	99.6 %
38b	$C_{15}H_{11}Cl_2N_3O$	319.03	320.13	318.04	DAD (λ_{max} = 238 nm)	95.5 %
40	$C_{14}H_9Cl_2N_3O$	305.01	306.31	304.06	DAD	99.0 %

					(λ_{max} = 230 nm)	
41	$C_{14}H_9Cl_2N_3O$	305.01	306.33	304.07	DAD (λ_{max} = 232 nm)	98.4 %
42	$C_{14}H_9F_2N_3O$	273.07	274.33	271.93	DAD (λ_{max} = 230 nm)	99.1 %
43	$C_{14}H_9ClFN_3O$	289.04	290.30	288.11	DAD (λ_{max} = 232 nm)	99.4 %
44	$C_{14}H_9ClFN_3O$	289.04	290.27	288.05	DAD (λ_{max} = 234 nm)	99.4 %
45	$C_{16}H_{15}N_3O_3$	297.11	298.47	296.30	DAD (λ_{max} = 228 nm)	99.9 %
46	$C_{15}H_{12}ClN_3O_2$	301.06	302.21	300.18	DAD (λ_{max} = 226 nm)	99.9 %
47	$C_{14}H_{10}ClN_3O_2$	287.05	288.10	286.10	DAD (λ_{max} = 226 nm)	98.5 %
48	$C_{15}H_{12}ClN_3O_2$	301.06	302.19	300.19	DAD (λ_{max} = 230 nm)	99.5 %
49	$C_{14}H_{10}ClN_3O_2$	287.05	288.10	286.09	DAD (λ_{max} = 226 nm)	99.3 %
53	$C_{15}H_{10}Cl_2N_2O$	304.02	305.17	303.11	DAD (λ_{max} = 238 nm)	95.1 %
54	$C_{16}H_{12}Cl_2N_2O$	318.03	319.14	317.09	DAD (λ_{max} = 242 nm)	97.5 %
55	$C_{14}H_9Cl_2N_3O$	305.01	306.32	304.07	DAD (λ_{max} = 238 nm)	99.2 %
56	$C_{13}H_8Cl_2N_4O$	306.01	307.31	305.15	DAD (λ_{max} = 222 nm)	95.2%
58	$C_{14}H_9Cl_2N_3$	289.02	290.27	288.05	DAD (λ_{max} = 238 nm)	95.1 %
59	$C_{15}H_{11}Cl_2N_3$	303.03	304.12	302.14	DAD (λ_{max} = 240 nm)	97.4 %

Chemical stability of compounds 54 and 59

Control of chemical stability of the reference compound **54** and the test compound **59** was performed by measuring LC/ESI-MS spectra of 10 mM DMSO stock solutions after 70 days at room temperature and comparing the results with the corresponding original spectra of the pure compounds.

LC/ESI-MS stability control experiment

A volume of 5.0 µL of each 10 mM DMSO stock solution was injected into the Agilent 1100 HPLS system coupled with API 2000 mass spectrometer using a NUCLEODUR C18 Gravity HPLC column (50 × 2.0 mm, particle size 3.0 µm). The elution was performed with a gradient of water/methanol containing 2.0 mM ammonium acetate from 90:10 to 0:100 for 20 min total run time at a flow rate of 300 µL/mi, starting the gradient after 10 min for 10 min. UV absorption was detected from 220 to 400 nm using DAD.

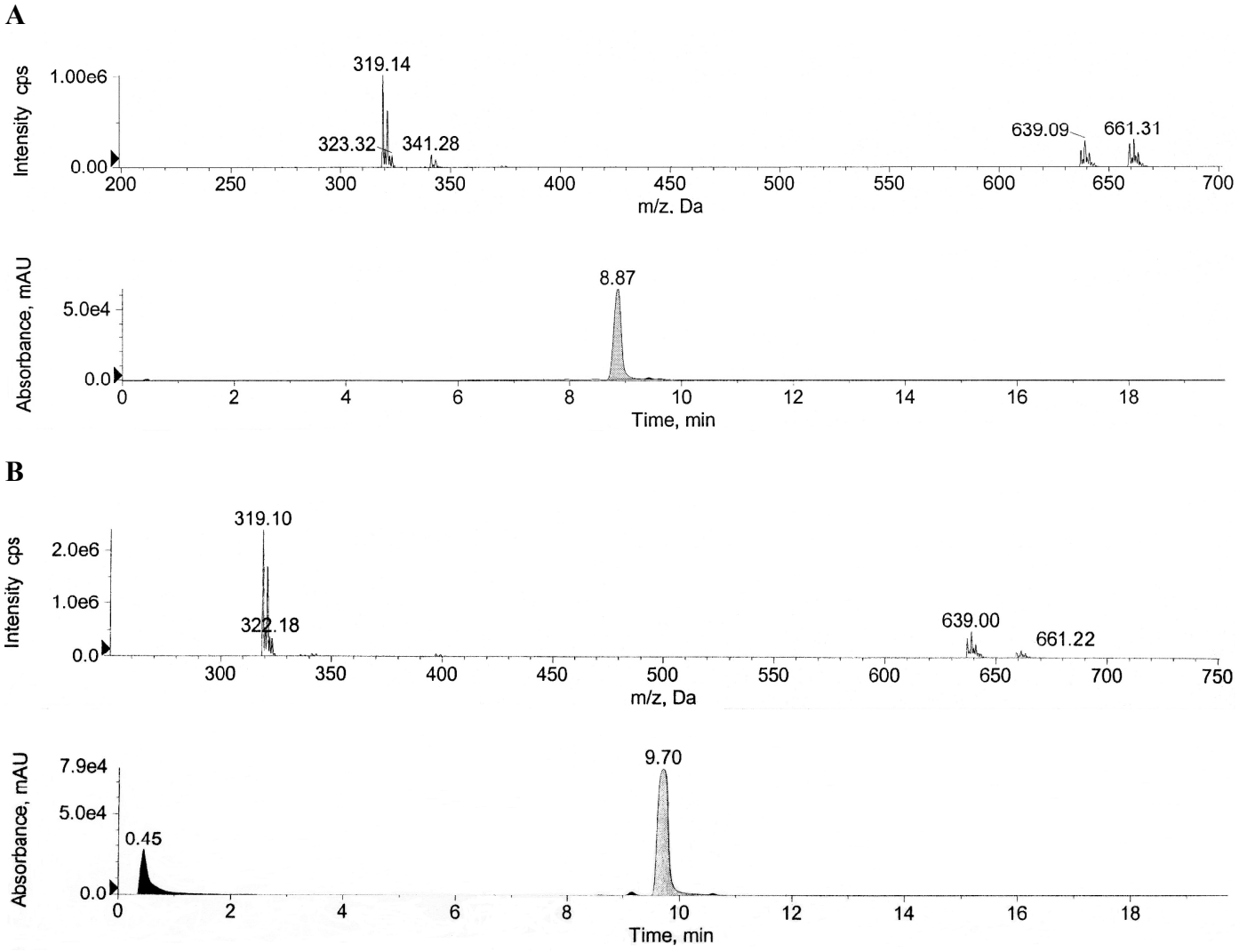

Figure S3. Comparison of the mass spectra in positive mode (top) and the HPLC chromatogram (bottom) of **54** (M_R 318.03) after purification (**A**) measured with a standard gradient (H_2O/MeOH, 60:40 to 0:100, starting the gradient after 10 min for 10 min) and after 70 days (**B**) measured with stability control gradient (H_2O/MeOH, 90:10 to 0:100, starting the gradient after 10 min for 10 min). The area around 0.45–2.2 min is due to the solvent DMSO and was therefore not considered for calculating the purity. The difference in the observed retention times is due to the different HPLC gradients.

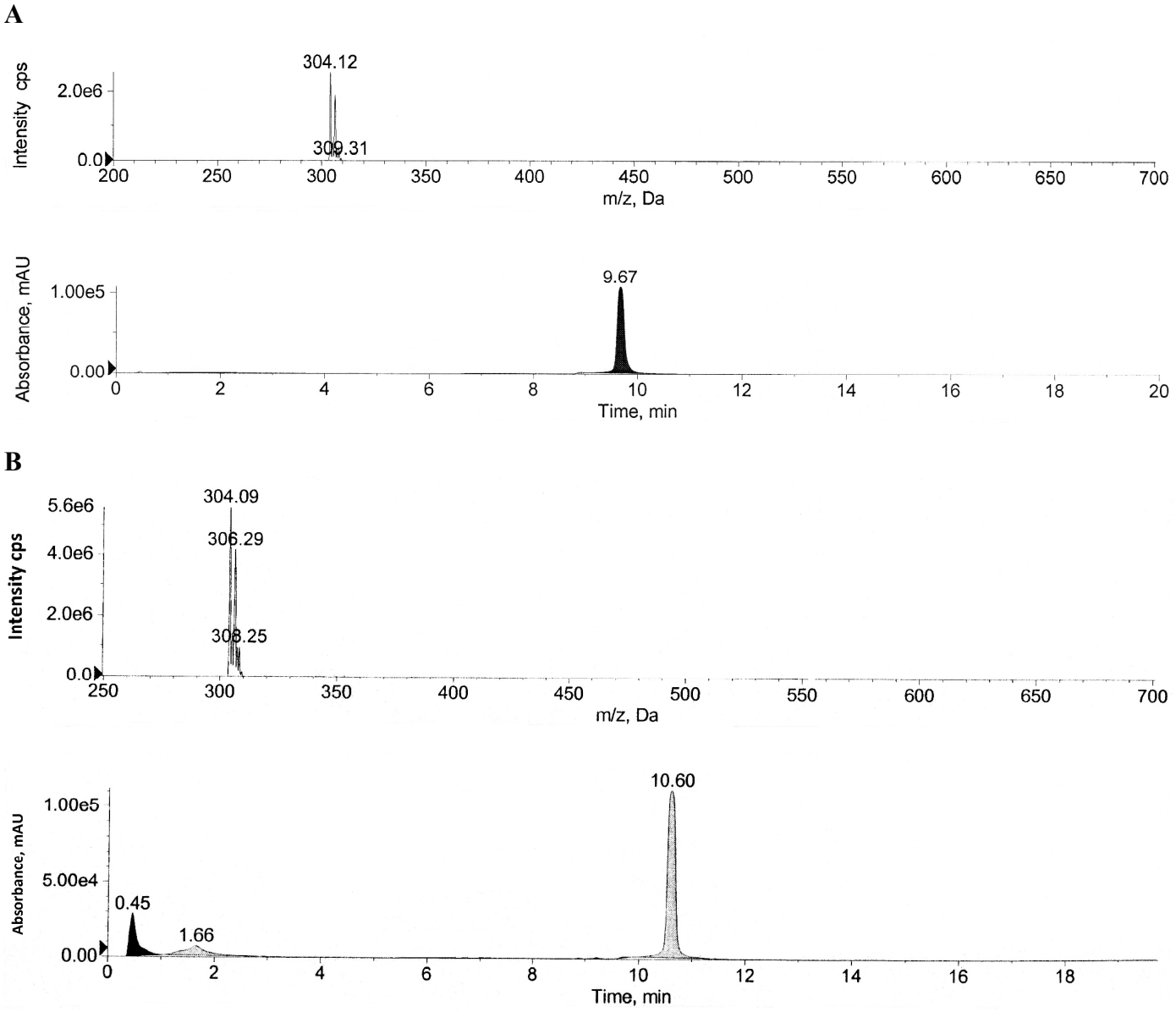

Figure S4. Comparison of the mass spectra in positive mode (top) and HPLC chromatogram (bottom) of **59** (M_R 303.03) after purification (**A**) measured with a standard gradient (H_2O/MeOH, 60:40 to 0:100, starting the gradient after 10 min for 10 min) and after 70 days (**B**) measured with stability control gradient (H_2O/MeOH, 90:10 to 0:100, starting the gradient after 10 min for 10 min). The area around 0.45–2.5 min is due to the solvent DMSO and was therefore not considered for calculating the purity. The difference in the observed retention time is due to the different HPLC gradients.

Table S2. Purity of compounds **54** and **59** determined by LC-MS.

Compd	Determination period	Retention time (min)	Gradient (H_2O : MeOH)	Purity (%)
54	0 h	8.87	60 : 40	97.7
54	70 d	9.70	90 : 10	96.6
59	0 h	9.67	60 : 40	97.4
59	70 d	10.6	90 : 10	84.7

E/Z isomery of compound 58

It is well known that under standard conditions the *E*-isomers are energetically more stable than their *Z*-diastereomers. For a better understanding of the relationship between the bioactivity at the configurational ground state (e.g., *E* versus *Z* isomers) and isomeric stability of class III MAO-B inhibitors, the respective *E*-/*Z*-geometry of **58** was optimized using MMFF94 force field.[3] The best conformers for each isomer obtained after conformer distribution are presented in Figure S5.

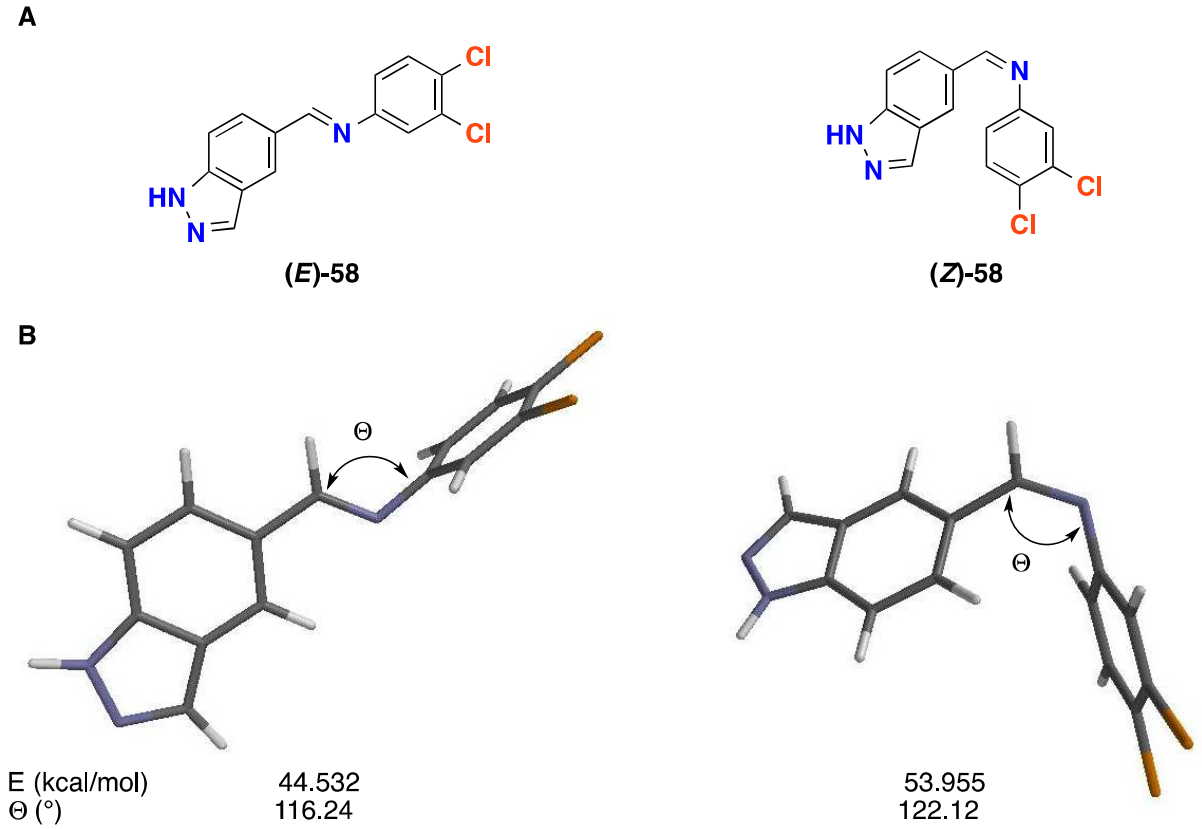

Figure S5. (**A**) *E*/*Z*-stereoisomers of **58**: **(*E*)-58** is energetically more favorable compared to **(*Z*)-58**. (**B**) Lowest energy geometries for the corresponding conformers and pertinent molecular parameters: the equilibrium energy E and dihedral angle Θ between the linker and phenyl ring. The dihedral angles between the 3,4-dichlorophenyl-ring plane and the indazole plane around the double bond are 87.38° for **(*E*)-58** and 72.11° for **(*Z*)-58**, respectively. Both molecular planes are orthogonal relative to each other, especially in the *E*-isomer. The energy values confirm the higher stability of *E*- versus *Z*-isomer of **58**. The respective geometries were drawn in Titan v.1.05.[3]

Pharmacological studies

Drugs and materials

The drugs, reagents and materials used in the MAO experiments were the new 37 target compounds, safinamide, *R*-(-)-deprenyl hydrochloride (Selegiline, purchased from Sigma-Aldrich M003), *N*-methyl-*N*-propargyl-3-(2,4-dichlorophenoxy)-propylamine hydrochloride (clorgyline, Sigma-Aldrich M3778), dimethyl sulfoxide (DMSO, Rotipuran® ≥ 99.8 % p.a., Roth 4720), 7-hydroxy-3*H*-phenoxazin-3-one (resorufin, dye content 95 %, Sigma-Aldrich 424455), *p*-tyramine hydrochloride (content 98 %, Alfa Aesar A12220), *di*-sodium hydrogen phosphate heptahydrate (Applichem A6292), sodium *di*-hydrogen phosphate monohydrate (≥ 98.0 % p.a., Roth K300.1), reconstituted horseradish peroxidase (HRP 200 U/mL, Sigma-Aldrich P6782), and Amplex® Red MAO assay kit (Invitrogen A12214). The human recombinant monoamine oxidase enzymes (microsomes of baculovirus-infected insect cells) were purchased from commercially sources (isoform MAO-A, Sigma-Aldrich M7316; isoform MAO-B, Sigma-Aldrich M7441). Rat MAO enzyme preparations were prepared as described in the article.

Preparation of buffer and stock solutions for MAO assays

The appropriate dilutions of the above drugs were freshly prepared before use in deionized water (Purelab flex, ELGA Labwater LLC, Woodridge, USA) and kept at -20 °C. The following concentrated stock solutions were used: *R*-(-)-deprenyl hydrochloride (selegiline), clorgyline (0.5 mM) and resorufin sodium salt (2.0 mM) in deionized water. The stock solutions were prepared by adding of 1.0 mL H_2O directly into the individual vials.[4] In all assays, no significant pharmacological effects of deionized water and DMSO were observed.

Preparation of sodium phosphate buffer

Sodium phosphate buffer solution 50 mM was prepared by dissolving 10.4 g of *di*-sodium hydrogen phosphate heptahydrate and 1.56 g of monosodium *di*-hydrogen phosphate each in 100 mL of deionized water. Both solutions were combined, diluted to a final volume of 1000 mL with deionized water and adjusted at pH 7.4. The solution was sterilized by autoclaving.

p-Tyramine hydrochloride stock solution

p-Tyramine hydrochloride was prepared as a 100 mM stock solution in deionized water and stored at -20 °C.

Horseradish peroxidase (HPR) solution

For the preparation of HPR solution were used 200 U/mL of the HPR enzyme diluted in 50 mM phosphate buffer at pH 7.4; the solution was stored at -20 °C.

Amplex Red Reagent[4]

A 20 mM stock solution of Amplex Red reagent used in the MAO assays was freshly prepared by dissolving 1.0 mg of the powdered dye component in 200 µL of DMSO under ice water cooling. Due to its photosensitivity the Amplex® Red reagent solution must by light-protected before use.

Test compounds stock solutions

Depending on their molecular weight, test compounds were weighed and diluted in DMSO to prepare a 10 mM stock solution. A 1.0 mM test sample solution was prepared by a 1:10 dilution with DMSO.

Pharmacological data and statistical analysis

A one-step fluorimetric method for continuous detection was used to determine the activity of MAO enzymes in the absence and in the presence of a test compound.[5] Figure S6 illustrates the two-step reaction scheme of the MAO assay. Hydrogen peroxide is produced via an oxidative deamination reaction of *p*-tyramine used as a MAO substrate in the first reaction step A. The Amplex® Red reagent is a highly sensitive and stable substrate molecule for the horseradish peroxidase-catalyzed reaction converting hydrogen peroxide to water (step B in Figure S6).[4] To estimate the inhibitory effects of the test compounds and reference compounds on the corresponding MAO isoform enzymatic activity, we evaluated indirectly the production of hydrogen peroxide as a function of the fluorescence per unit of time (fluorescence arbitrary units/min), and subsequently the ratio/min of resorufin produced in the reaction between hydrogen peroxide and Amplex Red reagent. To prepare a standard curve we used several concentrations of resorufin ranging from 0 to 20 μM, where X = ratio of resorufin and Y = fluorescence arbitrary units. Therefore, the ratio of resorufin production is equal to the ratio of the substrate *p*-tyramine oxidized by MAO isoenzymes to 2-(4-hydroxyphenyl)acetaldehyde per minute in the two-step stoichiometric reaction (ratio *p*-tyramine oxidized/resorufin produced = 1:1).

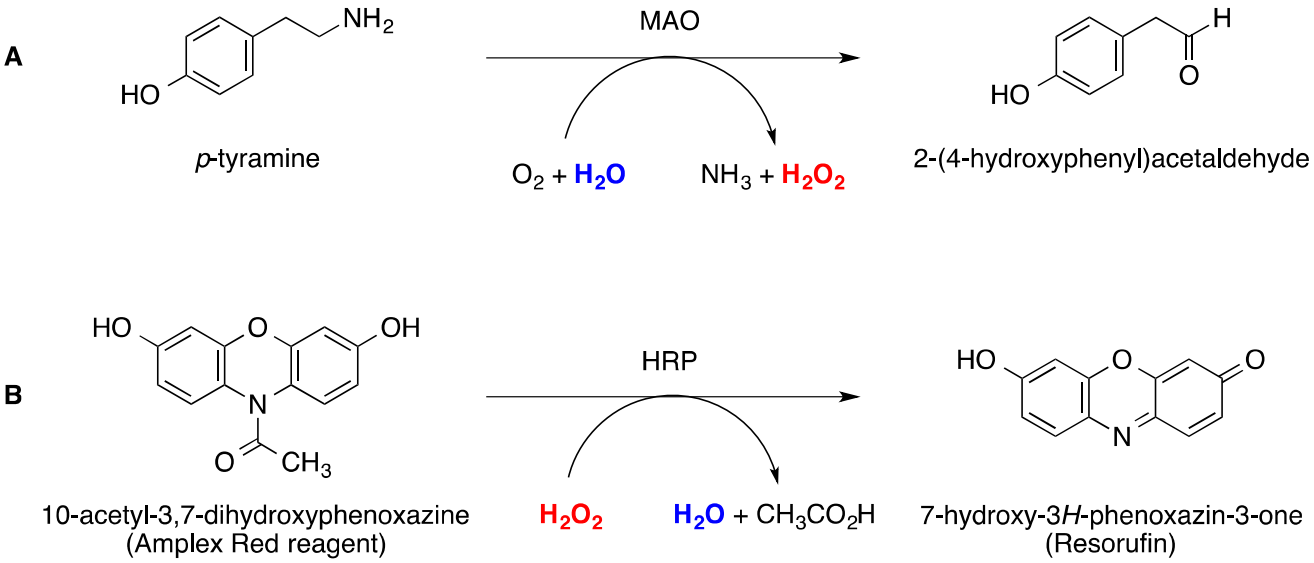

Figure S6. Two-step reaction scheme for the determination of MAO activity: Production of hydrogen peroxide (H_2O_2) via an oxidative deamination reaction of the substrate *p*-tyramine (step **A**) by MAO and subsequent HRP-catalyzed H_2O_2 oxidation of the Amplex® Red reagent (non-fluorescent) to the highly fluorescent resorufin (step **B**).[6–8]

The MAO-A inhibitor clorgyline and the MAO-B inhibitor *R*-(-)-deprenyl hydrochloride (selegiline) were used to determine the non-MAO-A and non-MAO-B enzyme activity, respectively, and subtracted from the total activity measured. The experiments were performed with different concentrations of clorgyline and selegiline (final concentrations 1.0 μM) to perform the corresponding concentration-response curves serving as a positive control. As a substrate of both MAO-A and MAO-B isoforms *p*-tyramine was used (final concentration 300 μM for the rat and 150 μM for the human MAO assays). The inhibitory activity of all tested drugs (37 new compounds plus reference inhibitors) is expressed as IC_{50} values corresponding to the concentration of these compounds required for 50% reduction of the control MAO isoform enzyme activity. The IC_{50} values were estimated by non-linear regression (curve fit) using GraphPad Prism Version 4.0 software (San Diego, CA, USA).[9] The initial standard screening concentration for each test compound was 10 μM followed by a concentration of 0.1 μM, if the tested compound showed significant inhibitory activity, followed by the determination of full concentration-inhibition curves for all active compounds.

Sigmoidal dose-response equation 1 (variable slope) was used to fit the dose-response curve of each compound and reference inhibitor:

(1) $$Y = Bottom + (Top - Bottom) / (1+10^{\Lambda}((LogEC_{50} - X)*HillSlope))$$

Where X is the logarithm of the tested compound molar concentration, Y is the response (i.e. corresponding percentage of inhibition control resorufin production obtained for each concentration), Bottom and Top is the bottom and the top of the curve, $LogEC_{50}$ represents the half-maximal inhibitory concentration of the tested compound for each experiment, and Hill´s Slope is the slope factor. This equation is also identical to the "four parameter logistic equation" where Y starts at the bottom and goes to the top with a sigmoid shape.[9] All assays were performed in triplicate for each tested new compound and for reference inhibitors and, if necessary, in quadruplicate (e.g., compound **53**). Figure S7 shows the experimental mean curves for compound **15** at the rat and the human MAO-B isoenzyme as an example.

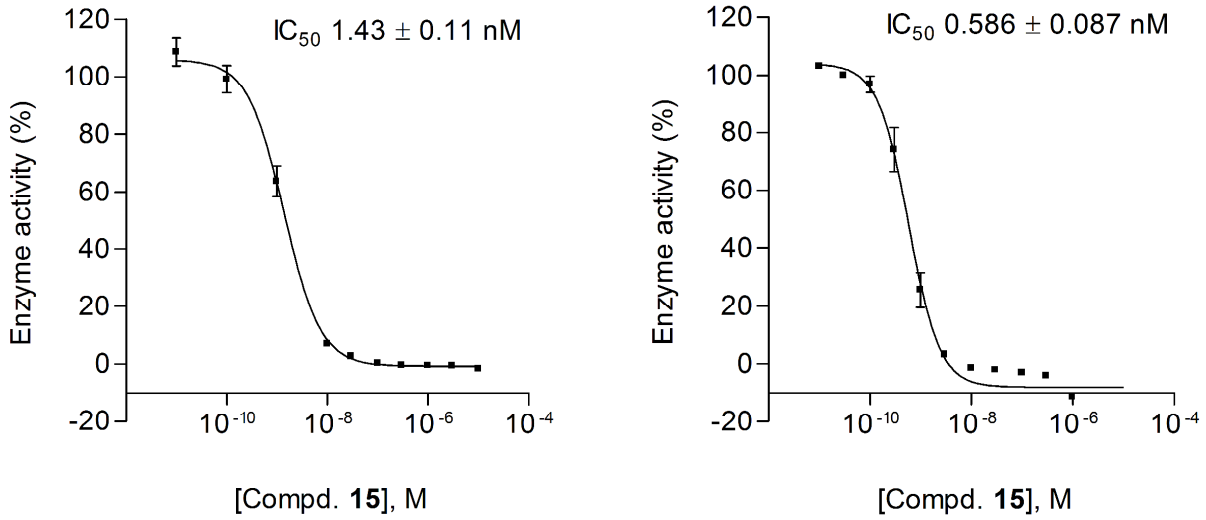

Figure S7. Mean inhibition curve for compound **15** at rat liver mitochondrial MAO-B pretreated with clorgyline (30 nM). Mean IC_{50} versus *p*-tyramine (300 µM) is 1.43 ± 0.11 nM (left). Mean inhibition curve for compound **15** at the human recombinant MAO-B enzyme. Mean IC_{50} versus *p*-tyramine (150 µM) is 0.586 ± 0.087 nM (right).

The nonlinear regression (curve fit) and linear regression were used to estimate the kinetic parameters (K_m and V_{max}) and the inhibition constant (K_i), respectively, of human MAO-B inhibition for compound **15** in the corresponding competitive experiments using GraphPad Prism Version 4.0 software (San Diego, CA, USA). Michaelis-Menten equation 2 was used to fit the double-reciprocal Lineweaver-Burk plots:

(2) $$Y = V_{max}*X / (K_m+X)$$

Where X is 1/*p*-tyramine molar concentration, Y is 1/reaction velocity (V), V_{max} is the maximal velocity saturation, and K_m is the substrate concentration required to reach half-maximal velocity (Michaelis constant, $V_{max}/2$). Equation 3 was used to give the relationship between the rates of the reaction velocity (V) and the inhibitor concentration at each substrate concentration:

(3) $$Y = \frac{K_m * X}{V_{max} * [S] * K_i} + \frac{1}{V_{max}}(1 + \frac{K_m}{[S]}$$

Where X is the inhibitor concentration of **15** (in nM), Y is 1/reaction velocity (1/v), V_{max} is the maximal velocity saturation, K_m is the Michaelis constant, and [S] is the substrate concentration.

Rat versus human MAO-B activity of selected compounds

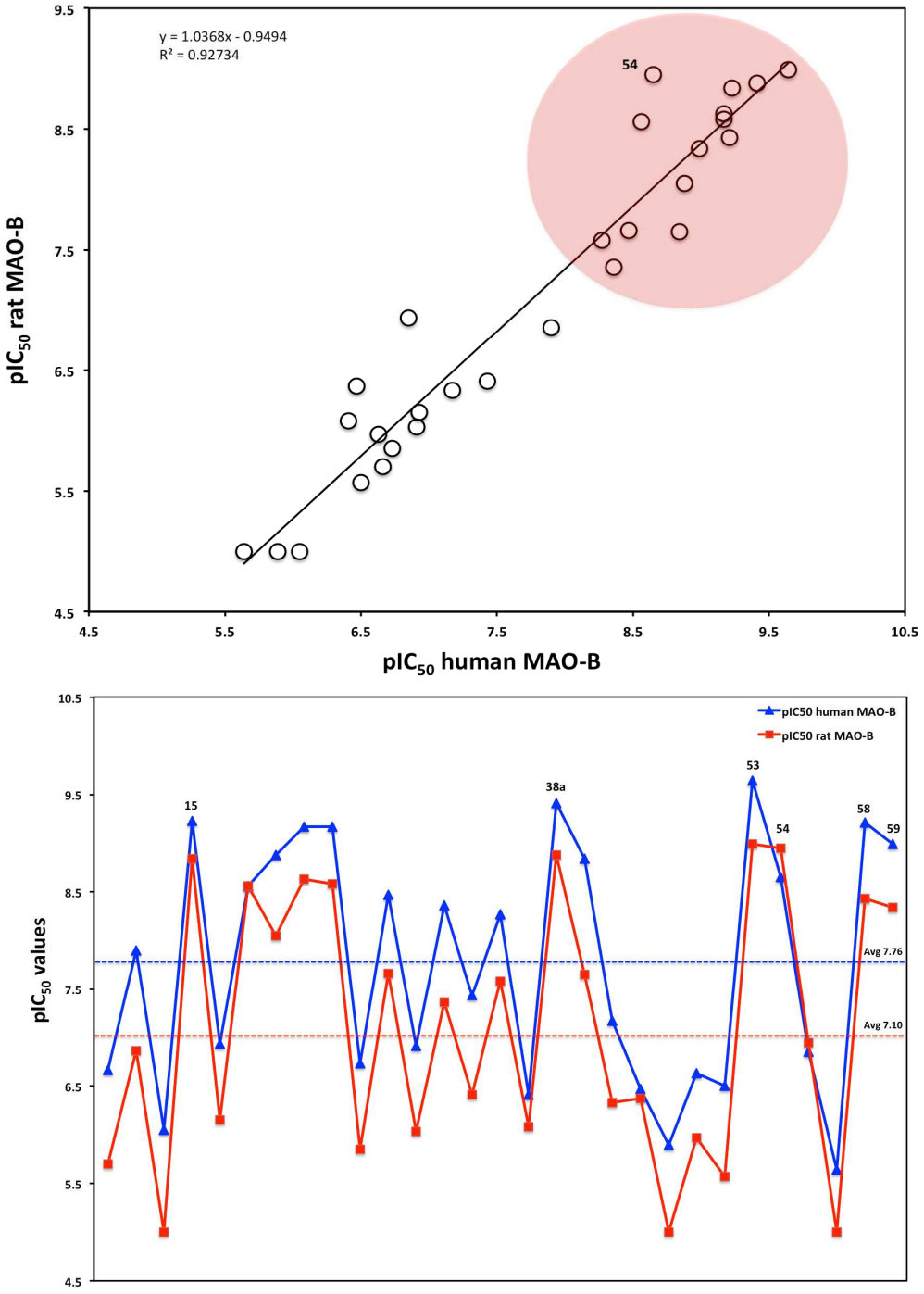

Figure S8. Square plot of pIC_{50} values at human compared to rat MAO-B determined for the 29 most potent compounds (top). Top-right corner contains highly potent and selective class I, II and III MAO-B inhibitors (coral pink circumscribed circle). Correlation chart of pIC_{50} values at human and rat MAO-B determined for the 29 most potent compounds (**B**). The average pIC_{50} values at rat (red dashed line/red squares) and human (blue dashed line/blue triangles) MAO-B are indicated (avg. pIC_{50} 6.70 at rat MAO-B, avg. pIC_{50} 7.22 at human MAO-B). The highly potent and selective MAO-B inhibitors are highlighted.

Dixon plot for compound 15

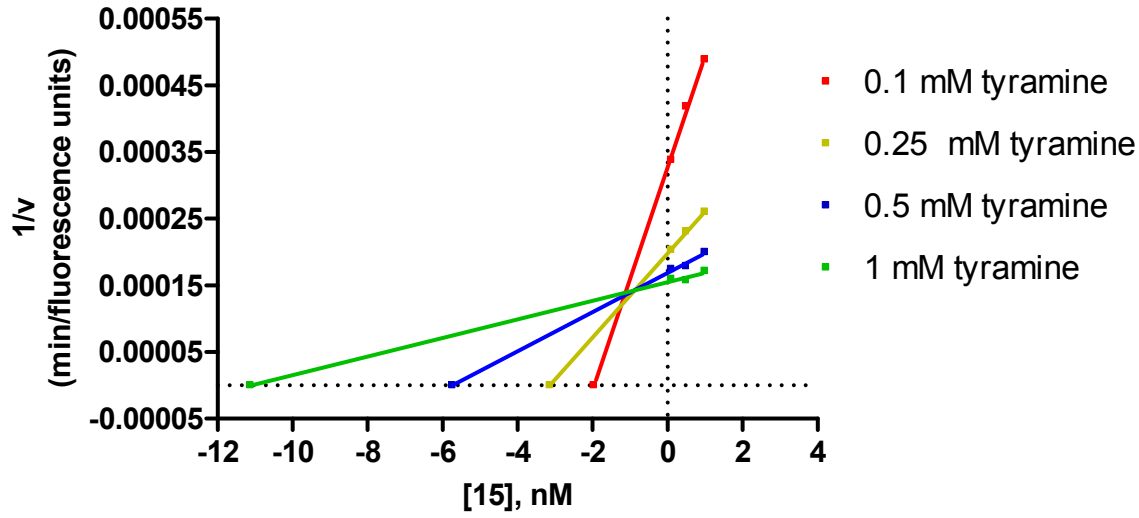

Figure S9. Dixon plot of the inhibition of recombinant human MAO-B enzyme by different concentrations of compound **15** (0.1, 0.5, 1 nM) in the presence of the substrate *p*-tyramine (0.1, 0.25, 0.5, 1 mM). Reciprocal MAO-B inhibitory activity was plotted against the inhibitor concentration. From the intersection a K_i value of 0.864 nM was calculated which is in the same range as the determined IC_{50} value (0.586 ± 0.087 nM).

Physicochemical properties of the synthesized compounds

The physicochemical parameters **(**Table S3) of the target compounds including their molecular weight (M_R), octanol-water partition/distribution coefficients (clogP/clog$D_{7.4}$), topological polar surface area (*t*PSA), strongest basic/acidic pK_a values, hydrogen bond donor/acceptor (HBD/HBA) counts, rotatable bonds (Rot.), and heavy atoms (HA) were calculated by the Instant JChem program (ChemAxon, Version 6.0.2, 2013).[10]

Table S3. Selected physicochemical properties of the synthesized compounds calculated by Instant Jchem software and determined melting points (M.p.)

Compd	M_R	clogP	clog$D_{7.4}$	*t*PSA (Å^2)	p*K*a	HBD	HBA	Rot.	HA	M.p. (°C)
10	357.8	2.26	2.26	83.1	3.0 / 11.2	2	5	3	25	238.1–239.1
11	268.3	0.43	0.43	78.1	1.2 / 13.3	2	2	2	20	247.2–248.6
12	289.7	3.13	3.13	57.8	1.2 / 10.0	2	2	2	20	269.8–270.5
13	306.1	3.60	3.60	57.8	1.2 / 10.7	2	2	2	20	264.7–265.3
14	306.1	3.60	3.60	57.8	1.2 / 11.1	2	2	2	20	277.5–277.6
15	306.1	3.60	3.60	57.8	0.8 / 11.0	2	2	2	20	270.8–271.6
16	320.2	3.58	3.58	57.8	1.2 / 13.3	2	2	3	21	269.2–274.3
26	237.3	2.39	2.39	57.8	0.8 / 12.0	2	2	2	18	284.8–285.3
27	306.1	3.60	3.60	57.8	0.8 / 10.5	2	2	2	20	302.7–304.8
28	289.7	3.13	3.13	57.8	0.8 / 10.9	2	2	2	20	239.9–241.2
29	289.7	3.13	3.13	57.8	0.8 / 10.7	2	2	2	20	246.9–247.9
30	273.2	2.67	2.67	57.8	0.8 / 10.5	2	2	2	20	238.9–239.7
31	297.3	2.07	2.07	76.2	0.8 / 11.4	2	4	4	22	258.3–261.3
32	301.7	2.83	2.83	67.0	0.8 / 11.2	2	3	3	21	276.2–277.8
33	287.7	2.69	2.57	78.0	0.8 / 7.9	3	3	2	20	272.2–273.4
34	301.7	2.83	2.83	67.0	0.8 / 11.3	2	3	3	21	279.6–281.6
35	287.7	2.69	2.50	78.0	0.8 / 7.7	3	3	2	20	306.6–307.3
36	307.1	2.60	2.60	70.7	0.8 / 10.2	2	3	2	20	>320.5
37	320.2	3.30	3.30	57.8	0.9 / 13.1	2	2	3	21	204.8–205.6
38a	320.2	3.72	3.72	46.9	0.7 / 11.0	1	2	2	21	193.2–194.3
38b	320.2	4.08	4.08	46.9	0.8 / 11.0	1	2	2	21	180.7–181.6
40	306.1	3.60	3.60	57.8	0.9 / 10.0	2	2	2	20	272.3–273.5
41	306.1	3.60	3.60	57.8	0.9 / 9.9	2	2	2	21	277.4–278.6
42	273.2	2.67	2.67	57.8	0.9 / 9.9	2	2	2	20	264.8–265.5
43	289.7	3.13	3.13	57.8	1.0 / 10.0	2	2	2	20	257.8–258.3
44	289.7	3.13	3.13	57.8	1.0 / 10.0	2	2	2	20	280.9–281.3
45	297.3	2.07	2.07	76.2	1.0 / 10.1	2	4	4	22	204.4–205.4
46	301.7	2.83	2.83	67.0	1.0 / 10.0	2	3	3	21	159.6–160.6
47	287.7	2.69	2.57	78.0	1.0 / 7.9	3	3	2	20	263.8–264.6
48	301.7	2.83	2.83	67.0	1.0 / 10.1	2	3	3	21	156.1–156.9
49	287.7	2.69	2.50	78.0	1.0 / 7.7	3	3	2	20	257.2–258.3
53	305.2	4.37	4.37	44.9	-3.9 / 11.0	2	1	2	20	233.8–234.8
54	319.2	4.60	4.60	34.0	-3.9 / 11.0	1	1	2	21	178.9–180.3
55	306.2	3.06	3.04	46.4	6.1 / 10.9	1	2	2	20	267.7–268.9
56	307.1	2.10	2.10	59.3	2.5 / 10.7	1	3	2	21	326.3–327.3
58	290.2	4.38	4.38	41.0	2.1 / 13.4	1	2	2	19	207.1–207.5
59	304.2	4.50	4.50	30.2	2.1	0	2	2	20	145.7–146.2

The physicochemical parameters (Table S4) of the target compounds including their molar volume (V_m), water solubility (S_w) and log(1/S_w) were calculated by the ACD/ChemSketch program (ACD Labs, Ver. 12.0, 2013).[11]

Table S4. Mean melting points (MP) and selected physicochemical properties of the synthesized compounds calculated by the ACD/ChemSketch software

Compd	V_m ± SEM (cm^3/mol)	S_w (g/L)[a]	log(1/S_w)[b] (mol/L ± 1.0)	MP (°C)
10	242.4 ± 3.0	1.13	2.5	238.6
11	182.8 ± 3.0	3.87	1.8	247.9
12	190.1 ± 3.0	24.6	1.1	270.2
13	197.8 ± 3.0	$2.2x10^{-3}$	5.2	265.0
14	197.8 ± 3.0	$79x10^{-3}$	3.6	277.6
15	197.8 ± 3.0	$22x10^{-3}$	4.1	271.2
16	212.7 ± 3.0	0.12	3.4	271.8
26	173.9 ± 3.0	3.37	1.8	285.1
27	197.8 ± 3.0	$13x10^{-3}$	4.4	303.8
28	190.1 ± 3.0	$85x10^{-3}$	3.5	240.6
29	190.1 ± 3.0	$85x10^{-3}$	3.5	247.4
30	182.3 ± 3.0	0.36	2.9	239.3
31	221.9 ± 3.0	4.06	1.9	259.8
32	209.9 ± 3.0	$1.2x10^{-3}$	5.4	277.0
33	184.3 ± 3.0	2.09	2.2	272.8
34	209.9 ± 3.0	0.19	3.2	280.6
35	184.3 ± 3.0	$4.0x10^{-3}$	5.3	307.0
36	191.0 ± 3.0	$0.21x10^{-3}$	6.2	320.0
37	220.0 ± 3.0	0.22	3.2	205.2
38a	223.8 ± 3.0	$17x10^{-3}$	4.3	193.8
38b	223.8 ± 7.0	$23x10^{-3}$	4.1	181.2
40	197.8 ± 3.0	$22x10^{-3}$	4.2	272.9
41	197.8 ± 3.0	$53x10^{-3}$	6.8	278.0
42	182.3 ± 3.0	0.37	2.9	265.2
43	190.1 ± 3.0	0.085	3.5	258.1
44	190.1 ± 3.0	$85x10^{-3}$	3.5	281.1
45	221.9 ± 3.0	4.06	1.9	204.9
46	209.9 ± 3.0	0.31	3.0	160.1
47	184.3 ± 3.0	2.09	2.2	264.2
48	209.9 ± 3.0	0.19	3.2	156.5
49	184.3 ± 3.0	0.97	2.6	257.8
53	204.6 ± 3.0	$8.8x10^{-3}$	4.5	234.2
54	235.1 ± 3.0	$3.0x10^{-3}$	5.0	179.6
55	208.5 ± 7.0	$65 x10^{-3}$	3.7	268.3
56	197.2 ± 7.0	0.41	2.9	326.8
58	205.2 ± 7.0	0.67	2.6	207.3
59	226.5 ± 7.0	$37x10^{-3}$	3.9	146.0

[a]The solubility at 25°C in water (pH 7.4) was calculated based on the corresponding mean melting point (MP) of the compound. [b]log(1/S_w) values were calculated using aqueous solubility (S_w): log(1/S_W) = S_w/M_R, where M_R is the relative molar mass of the target compound.

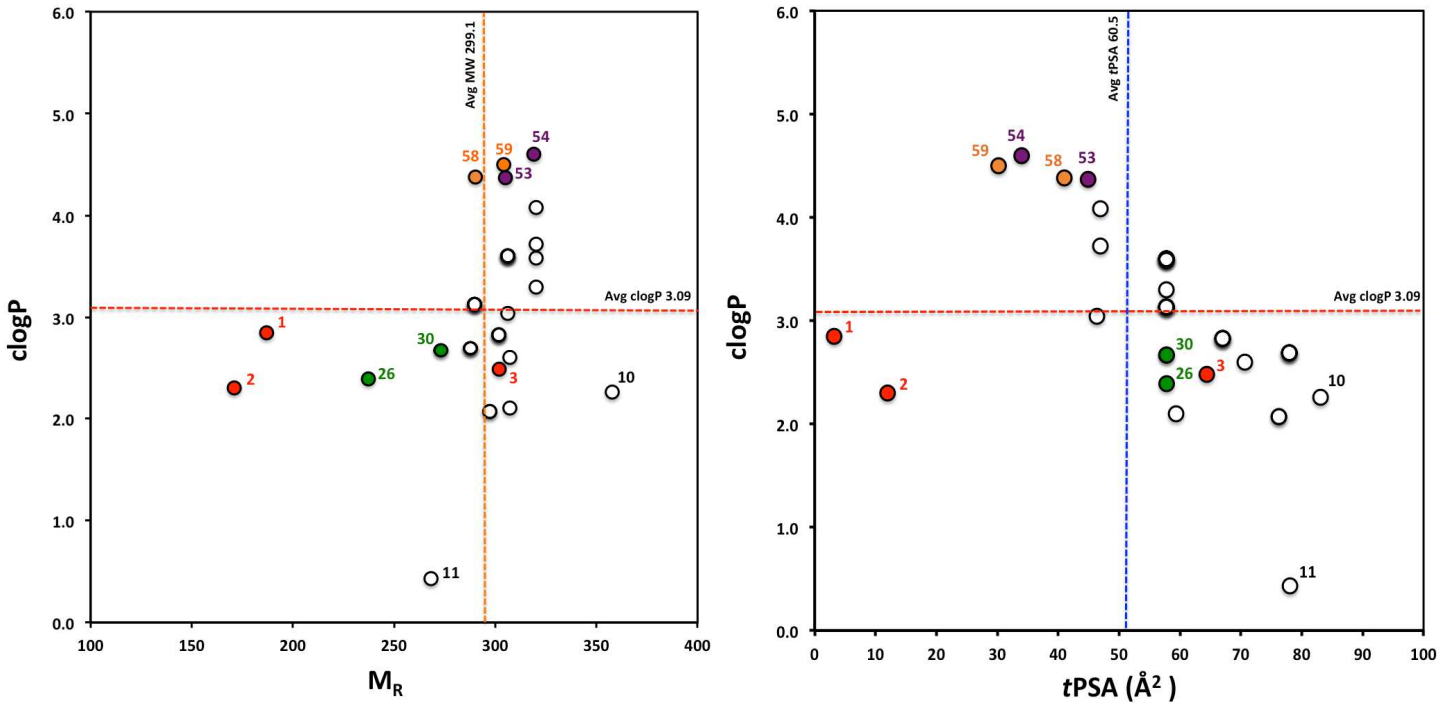

Figure S10. Distribution of the clogP values for all target compounds plotted versus molecular weight (M_R) (left) and *t*PSA in Å^2 (right). The reference drugs and selected compounds are indicated in red (**1**, **2** and **3**), green (indazole-5-carboxamides **26** and **30**, class I), violet (indole-5-carboxamides **53** and **54**, class II) and orange (indazol-5-yl)methanimines **58** and **59**, class III), respectively. The red dashed line represents the average value for clogP (3.09), while the orange and blue dashed lines show the average values for M_R (299.1) and *t*PSA (60.5 Å^2), respectively. Compounds **10** and **11** deviated from the average values of M_R and *t*PSA, while highly potent class II (**53** and **54**) and class III (**58** and **59**) MAO-B inhibitors are lipophilic (clogP > 4.0). Most of the synthesized compounds are considered to have suitable physicochemical parameters for oral bioavailability and a low risk for adverse effects related to high lipophilicity (logP 2-4, M_R < 400 and *t*PSA 50-90 Å^2).[12] The octanol/water partition coefficient clogP values were calculated as a measure of molecular hydrophobicity using a modified atom-based algorithm.[13] The final logP value of the target molecule is composed of the increment values of its atoms present in the molecule (atom contributions).[13,14]

A number of physicochemical properties such as lipophilicity/hydrophilicity (logP and logD at pH 7.4), number of hydrogen bond donors (HBD), (topological) polar surface area (*t*PSA), and molecular size and shape (depends on the number of heavy atoms and molecular weight) have been identified as most important factors that influence blood-brain barrier (BBB) permeability.[15] Table S5 provides suggested and preferred physicochemical property limits/ranges for increasing the potential for BBB penetration while considering the DMPK profile. Table S5 indicates also that the mean values for the physicochemical properties of the top-selling 25 CNS drugs (ranking of 2004) and the target compounds (this paper) are in the suggested limits.[15] Therefore, the physicochemical properties (except the HBD values with 19%) of the synthesized compounds reported in this paper are in the preferred ranges for compounds with high probability of CNS penetration.

Table S5. Comparison of suggested and preferred physicochemical property ranges for the top 25 CNS drugs[15] and the synthesized compounds (this paper).

Property	Mean values		Suggested limits	% of compounds in suggested limits		Preferred range	% of compounds in preferred range	
	Top 25 drugs[15]	Compd´s this paper		Top 25 drugs[15]	Compd´s this paper		Top 25 drugs[15]	Compd´s this paper
clogP	2.8	3.1	2–5	68	100	2–4	52	84
$clogD_{7.4}$	2.1	3.1	2–5	61	100	2–4	61	84
HBD	0.8	1.4	< 3	100	89	0–1	92	19
*t*PSA (Å^2)	47	60.1	< 90	96	100	< 70	76	76
M_R	293	299	< 500	100	100	< 450	100	100

The bioavailability, lead-likeness and rule-of-3 were evaluated using the Instant JChem software (ChemAxon, Version 6.0.2, 2013).[10] Compound **30** was evaluated positive regarding the three important criteria for CNS drug candidates.

Table S6. Evaluated properties of selected compounds as potential CNS drug candidates.

Compd.	MAO-B inhibitors[a]	Predicted bioavailability[b]	Lead-likeness[c]	Rule-of-3[d]
15	Class I	+	+	M_R 306.1 clogP 3.60
27	Class I	+	+	M_R 306.1 clogP 3.60
28	Class I	+	+	clogP 3.13
29	Class I	+	+	clogP 3.13
30	Class I	+	+	+
32	Class I	+	+	M_R 301.7 *t*PSA 67
34	Class I	+	+	M_R 301.7 *t*PSA 67
36	Class I	+	+	M_R 307.1 *t*PSA 70.7
38a	Class I	+	+	M_R 320.2 clogP 3.72
38b	Class I	+	clogP 4.08	M_R 320.2 clogP 4.08
53	Class II	+	clogP 4.37	M_R 305.2 clogP 4.37
54	Class II	+	clogP 4.60	M_R 319.2 clogP 4.60
58	Class III	+	clogP 4.38	clogP 4.38
59	Class III	+	clogP 4.50	M_R 304.2 clogP 4.50

[a]MAO-B inhibitors: indazole-5-carboxamides (class I), indole-5-carboxamides (class II), and (indazol-5-yl)methanimines (class III). [b]Criteria for oral bioavailability: $M_R \leq 500$, logP ≤ 5, donor counts ≤ 5, acceptor counts ≤ 10, rotatable bond counts ≤ 10, PSA ≤ 200, fused aromatic ring counts ≤ 5. [c]Criteria for lead likeness: $M_R \leq 450$, $\log D_{7.4} \geq -4$ and ≤ 4, ring counts ≤ 4, rotatable bond counts ≤ 10, donor counts ≤ 5, acceptor counts ≤ 8. [d]Rule-of-3: $M_R \leq 300$, logP ≤ 3, acceptor counts ≤ 3, rotatable bond counts ≤ 3, *t*PSA ≤ 60.[16]

Computational analysis

All ligand superposition computations were carried out with FlexS v.2.1.2 from BioSolveIT, Germany.[17,18] Default parameters were used throughout and the optimized base placement method was applied. Safinamide (**3**) in its crystal conformation (as extracted from PDB 2V5Z) served as the reference ligand. To avoid biasing, 3D starting conformations for the test ligands (compounds **15** and **30**) were generated with CORINA v.3.49 from Molecular Networks.[19-21] Gasteiger partial charges were used throughout.[22] The results are summarized in Table S7.

Table S7. Superposition results for reference safinamide (**3**) and selected ligands **15** and **30**.

Superposed ligand	Normalized FlexS Overlap Score	Normalized FlesS Volume Overlap	Absolute Overlap Volume [Å^3]
Safinamide (**3**)	1.000	1.00	1076.9
15	0.725	0.85	859.0
30	0.724	0.87	856.0

Figure S10 provides insight into the structural features of the newly designed indazole-5-carboxamides **15** and **30**. The overlay gives a hint to their higher MAO-B potency in comparison to safinamide (**3**). One sees the close matching of the Ar-Hal moieties, and also the backbones of **15** and **30** lie very well within the spatial region of the template **3**, the N2 positions of the indazole units matching the safinamide NH-group position almost exactly. In terms of the FlexS interaction-model similarities (reflecting donors, acceptors, delocalization, and amide character of the molecules), compounds **15** and **30** show a 72% and 75% identity, respectively. Owing to the somewhat smaller size of the test ligands, the volume overlaps reflect a spatial coverage of **3** in the range of 85%. This makes their high affinity even more striking. In addition, the superposition experiment supports the assumption of a relatively rare (compare Docking results) interplanar twist between the phenyl and indazole ring planes, enforcing a non-planarity between amide and at least one of the ring systems.

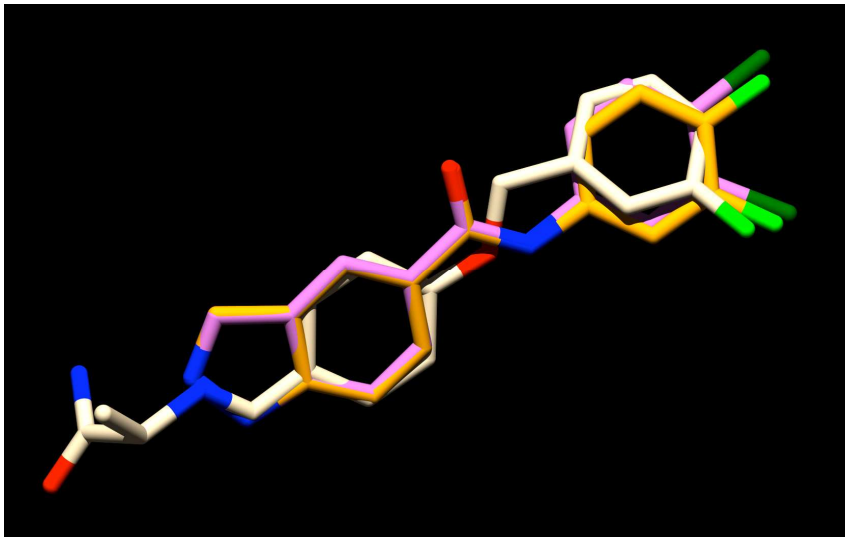

Figure S11. Compounds **15** (orange) and **30** (pink) overlaid onto the crystal structure of safinamide (**3**, off-white, PDB code 2V5Z; F atoms in light green, Cl in dark green). The 3D alignments have been computed with flexible ligands and safinamide as a template structure. Graphics were prepared with FlexV.[17]

REFERENCES

1 Colandrea, V. J.; Doherty, G. A; Hale, J. J.; Huo, P.; Legiec, I. E.; Toth, L.; Vachal, P.; Yan, L. (3,4-Disubstituted)propanoic carboxylates as S1P (EDG) receptor agonists. PCT Int. Appl. WO2005058848A1, 2005 (Merck & Co., Inc.).

2 Grima, P. M. P; Aguilar, N. I.; Mir, M. C.; Lopez, M. M. New 2-amidothiadiazole derivatives. PCT Int. Appl. WO2010043377 A1, 2010 (Allmirall, S.A.).

3 All conformer calculations were carried out using Titan v.1.05 software, 2000, Wavefunction Inc.

4 Product information for use of Amplex® Red Monoamine Oxidase Assay Kit (A12214), Molecular Probes – Invitrogen Detection Technologies, revised 01. October 2004.

5 Mohanty, J. G.; Jaffe, J. S.; Schulman, E. S.; Raible, D. G. A highly sensitive fluorescent micro-assay of H_2O_2 release from activated human leukocytes using a dihydroxyphenoxazine derivative. *J. Immunol. Methods* **1997**, *202*, 133–141.

6 Zhou, M.; Diwu, Z.; Panchuk-Voloshina, N.; Haugland, R. p. A stable non-fluorescent derivative of resorufin for the fluorometric determination of trace hydrogen peroxide: applications in detecting the activity of phagocyte NADPH oxidase and other oxidases. *Anal. Biochem.* **1997**, *253*, 162–168.

7 Towne, V.; Will, M.; Oswald, B.; Zhao, Q. Complexities in horseradish peroxidase-catalysed oxidation of dihydroxyphenoxazine derivatives: appropriate ranges for pH values and hydrogen peroxide concentrations in quantitative analysis. *Anal. Biochem.* **2004**, *334*, 290–296.

8 Gorris, H.; Walt, D. R. Mechanistic aspects of horseradish peroxidase elucidated through single-molecule studies. *J. Am. Chem. Soc.* **2009**, *131*, 6277–6282.

9 Miller, J. R. *GraphPad Prism Version 4.0 Step-by-Step Examples*, GraphPad Software Inc., San Diego CA, 2003.

10 Instant JChem v.6.0.2, ChemaAxon (http://www.chemaxon.com), 2013.

11 ACD/ChemSketch, v.12.0, Advanced Chemistry Development, Inc., Toronto, ON, Canada, http://www.acdlabs.com, 2013.

12 Wager, T. T.; Hou, X.; Verhoest, P. R.; Villalobos, A. Moving beyond rules: The development of a central nervous system multiparameter optimization (CNS MPO) approach to enhance alignment of druglike properties. *ACS Chem. Neurosci.* **2010**, *1*, 435–449.

13 Mannhold, R.; Van de Waterbeemd, H. Substructure and whole molecule approaches for calculating log*P*. *J. Comput.-Aided Mol. Des.* **2001**, *15*, 337–354.

14 Viswanadhan, V. N.; Ghose, A. K.; Revankar, G. R.; Robins, R. K. Atomic physicochemical parameters for three dimensional structure directed quantitative structure-activity relationships. 4. Additional parameters for hydrophobic and dispersive interactions and their application for an

automated superposition of certain naturally occurring nucleoside antibiotics. *J. Chem. Inf. Comput. Sci.* **1989**, *29*, 163–172.

15 Hitchcock, S. A.; Pennington, L. D. Structure-brain exposure relationships. *J. Med. Chem.* **2006**, *49*, 7559–7583.

16 Abad-Zapatero, C. Ligand efficiency indices for effective drug discovery. *Expert Opin. Drug Discov.* **2007**, *2*, 469–488.

17 FlexS/FlexV v.2.1.2, BioSolveIT GmbH, Germany, http://www.biosolveit.de, 2013.

18 Lemmen, C.; Lengauer, T.; Klebe, G. FlexS: A method for fast flexible ligand superposition. *J. Med. Chem.* **1998**, *41*, 4502–4520.

19 CORINA v.3.49, Molecular Networks GmbH, Erlangen, Germany, www.mol-net.de, 2014.

20 Sadowski, J.; Gasteiger, J. From atom and bonds to three-dimensional atomic coordinates: automatic model builders. *Chem. Rev.* **1993**, *93*, 2567–2581.

21 Sadowski, J.; Schwab, C. H. 3D Structure Generation and Conformational Searching. In *Computational Medicinal Chemistry and Drug Discovery*; Bultinck, P.; De Winter, H.; Langenaeker, W.; Tollenaere J. P.; Eds.; Dekker Inc.: New York; 2004; Vol. 30, pp 151–212.

22 Sadowski, J. Three-Dimensional Structure Generation: Automation. In *Encyclopedia of Computational Chemistry*; Schleyer, P. v. R.; Allinger, N. L.; Clark, T.; Gasteiger, J.; Kollman, P. A.; Schaefer, III, H. F.; Schreiner, P. R.; Eds.; John Wiley & Sons, Inc.: Chichester, UK; 1998; pp. 2976–2988.